PHYSICAL REVIEW A **71**, 063619 (2005)

Combined chips for atom optics

A. Günther,[1,*] M. Kemmler,[1] S. Kraft,[1] C. J. Vale,[2] C. Zimmermann,[1] and J. Fortágh[1]
[1]*Physikalisches Institut der Universität Tübingen, Auf der Morgenstelle 14, D-72076 Tübingen, Germany*
[2]*School of Physical Sciences, University of Queensland, Brisbane, Queensland 4072, Australia*
(Received 24 February 2005; published 30 June 2005)

We present experiments with Bose-Einstein condensates on a combined atom chip. The combined structure consists of a large-scale "carrier chip" and smaller "atom-optics chips," containing micron-sized elements. This allows us to work with condensates very close to chip surfaces without suffering from fragmentation or losses due to thermally driven spin flips. Precise three-dimensional positioning and transport with constant trap frequencies are described. Bose-Einstein condensates were manipulated with submicron accuracy above atom-optics chips. As an application of atom chips, a direction sensitive magnetic-field microscope is demonstrated.

DOI: 10.1103/PhysRevA.71.063619 PACS number(s): 03.75.Be, 03.75.Kk, 03.75.Lm, 34.50.Dy

I. INTRODUCTION

Interest in phase coherent experiments with ultracold quantum gases has motivated numerous theoretical and experimental investigations into microscopic magnetic traps [1]. An intriguing feature of microtraps is the possibility of constructing complex potentials using the magnetic field of microstructured conductors on a chip, as well as the precise spatial and temporal control of these potentials. Specific atom-optical experiments have been discussed, such as Bose-Josephson junctions in double well potentials [2], tunneling through a quantum dot in magnetic waveguides [3], or even scenarios for creating entangled pairs of atoms [4]. A central goal is the preparation of matter waves in microtraps with potential structures on the micron scale, comparable to the healing length of the condensate, which will allow for tunneling on experimentally viable time scales. Current experiments can readily produce Bose-Einstein condensates in magnetic microtraps [5,6], however, the potentials used to date have been too large scaled to reach the tunneling regime. To go beyond this, condensates must be moved closer to field generating elements, that is, to within a few microns of the chip surface.

With atom/conductor separations of a few microns, Johnson-noise induced spin-flip losses reduce the lifetime of the atomic cloud [7,8]. Furthermore, at distances extending to several tens of microns, irregularities of the trapping potential, arising from geometrical imperfections of the conductor [9] and the corresponding spatial fluctuation of magnetic field [10], cause fragmentation of atomic clouds.

In this paper we present a way to overcome these limiting surface effects which allows one to work at micron distances from the surface. A smooth waveguide potential is produced by a large scaled "carrier chip" situated several hundreds of microns from the surface of further "atom optics chips." At this distance, surface effects from the carrier are negligible [11]. The carrier chip is used for micropositioning a condensate. Attached to the surface of the carrier, additional atom-optics chips based on micron-scaled conductor patterns are used for steep and thin potential barriers. Due to the small amount of metal, Johnson-noise induced spin-flip rates are minimized even at close distances to the chip surface [12]. Since atoms are confined in a smooth waveguide and interact only with short sections of cross conductors at micron distances, stable conditions for coherent atom optics are achieved.

*URL: http://www.pit.physik.uni-tuebingen.de/zimmermann/; electronic address: aguenth@pit.physik.uni-tuebingen.de

II. THREE-DIMENSIONAL CONFINEMENT ON A CHIP

When manipulating condensates with micron-sized electromagnets, the exact position of the atoms with respect to these elements becomes crucial. Previous microtraps have used large external electromagnets to generate the so called bias field that is essential for the microtrap concept [13]. Because of the uncertainties in their geometry, accurate calculation of the trap parameters and position becomes difficult. In order to overcome this, we have developed a chip which includes all field generating elements necessary for three-dimensional confinement and manipulation. The microfabricated wire pattern defines a precise conductor geometry and the trap parameters and position can be computed with high accuracy. The conductor configuration was designed to provide three-dimensional positioning and transport of condensates, while keeping the trap frequencies constant.

A. Radial confinement and positioning

A magnetic waveguide potential can be realized by three parallel conductors as shown in Figs. 1(a) and 1(b). The magnetic field of the center conductor QP2, driven with a current of I_{QP2}, is superimposed with the bias field $\boldsymbol{B}_{\perp}$, generated by two other parallel conductors QP1 and QP3 ("quadrupole wires").

The inhomogeneous bias field is given by

$$\boldsymbol{B}_{\perp} = \frac{\mu_0}{2\pi}\left(\frac{I_{\mathrm{QP1}}y}{(d_{\mathrm{QP}}+x)^2+y^2} + \frac{I_{\mathrm{QP3}}y}{(d_{\mathrm{QP}}-x)^2+y^2}\right)\boldsymbol{e}_x - \frac{\mu_0}{2\pi}\left(\frac{I_{\mathrm{QP1}}(d_{\mathrm{QP}}+x)}{(d_{\mathrm{QP}}+x)^2+y^2} - \frac{I_{\mathrm{QP3}}(d_{\mathrm{QP}}-x)}{(d_{\mathrm{QP}}-x)^2+y^2}\right)\boldsymbol{e}_y. \quad (1)$$

d_{QP} is the distance between the conductors QP1 and QP2,

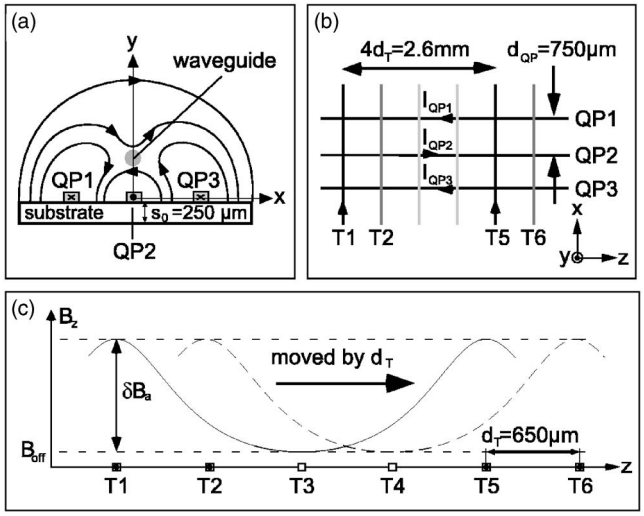

FIG. 1. (a) Three wire configuration on a chip used for a magnetic waveguide potential. The central conductor QP2 carries current opposite to the outer conductors QP1 and QP3. A waveguide is formed above the chip, as indicated by the magnetic-field lines. Marked also is the thickness of the substrate s_0=250 μm as used for the carrier chip in our experiment. (b) Conductor geometry for a microtrap with three-dimensional confinement. A waveguide potential is generated by the conductors QP1, QP2, and QP3. The magnetic field of a pair of perpendicular conductors T1 and T5 provide axial confinement with nonvanishing offset field. An equidistant set of perpendicular conductors ("transport conductors") can be used for an axial displacement. The geometry of conductors is marked: the distance between the QP wires d_{QP} is 750 μm and the distance between the transport wires is d_T=650 μm. (c) Translation of the trap. If the current in T1 and T5 is replaced by a current in T2 and T6, the trap is axially displaced by the distance of d_T=650 μm.

(and QP2 and QP3) and $I_{QPi}, i=1, 2,3$ are the respective currents. The waveguide forms in a line, where the bias field and the field of the central conductor cancel each other. This requires the current in the outer conductors to be opposite in direction to the current in the central conductor. We follow the convention that I_{QP2} is positive for currents in the $+z$ direction, and $I_{QP1/QP3}$ is positive in the $-z$ direction.

Applying the same current in QP1 and QP3, the y component of the bias field vanishes along the y axis, and the resulting bias field is

$$\boldsymbol{B}_\perp(x=0,y)=\frac{\mu_0}{\pi}\frac{yI_{QP1}}{d_{QP}^2+y^2}\boldsymbol{e}_x. \tag{2}$$

The waveguide forms at a distance of

$$y_0=d_{QP}\sqrt{\frac{1}{2I_{QP1}/I_{QP2}-1}} \tag{3}$$

on the y axis [Fig. 1(a)]. A trap is only formed if $|I_{QP1}| \geqslant |I_{QP2}/2|$. The radial field gradient a_r in the trap center of the three-wire configuration is given by

$$a_r=\frac{\mu_0}{2\pi}\frac{I_{QP2}}{y_0^2}\frac{2}{1+(y_0/d_{QP})^2}. \tag{4}$$

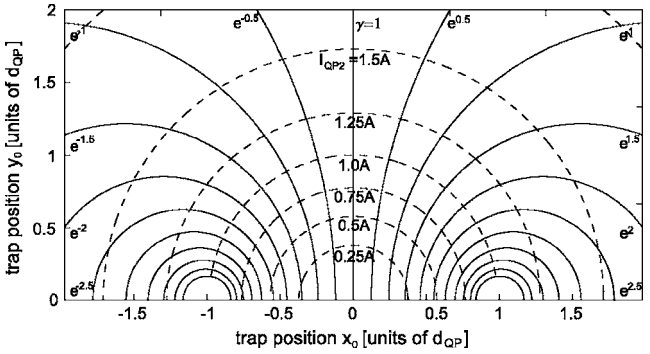

FIG. 2. Position of the waveguide in the x,y plane. Solid lines are trajectories for a constant ratio of $\gamma=I_{QP1}/I_{QP3}$ and increasing I_{QP2}. Dashed lines are trajectories for constant I_{QP2} and varying $\gamma=I_{QP1}/I_{QP3}$. The sum of the currents $I_{QP1}+I_{QP3}=2$ A was kept constant in this plot.

In the general case, the x,y position of the waveguide is determined by the currents I_{QP1}, I_{QP2}, and I_{QP3}:

$$x_0=\frac{d_{QP}}{2}\frac{I_{QP2}-I_{QP3}}{I_{QP1}+I_{QP2}+I_{QP3}},$$

$$y_0=\frac{d_{QP}}{2}\frac{[4I_{QP1}I_{QP3}-(I_{QP1}+2I_{QP2}+I_{QP3})^2]^{1/2}}{I_{QP1}+I_{QP2}+I_{QP3}}. \tag{5}$$

The trap can be positioned within a large area above the chip by changing the currents I_{QP1}, I_{QP3}, and I_{QP2}. Figure 2 shows trajectories corresponding to a constant ratio of I_{QP1} and I_{QP3} (solid lines) and constant I_{QP2} (dashed lines) while keeping the sum $I_{QP1}+I_{QP3}$ at a constant current of 2 A. The values are realistic for experiments discussed later.

B. Axial confinement and translation of the trap center

The waveguide produced by the three conductors will suffer from Majorana spin flips [14] because the magnetic field vanishes in the center of the waveguide. However, a magnetic offset field $\boldsymbol{B}_{off}$ along the symmetry axis, stabilizes the trap against these losses. The nonzero absolute value of the magnetic field $\boldsymbol{B}_{off}$ in the trap center also changes the radial potential shape from linear to parabolic [15]. The radial confinement is then characterized by the oscillation frequency $\omega_r=\sqrt{g_F\mu_B m_F/mB_{off}}a_r$, with the Landé factor g_F, the Bohr magneton μ_B, the magnetic quantum number m_F, and m the mass of the atom. To allow for three-dimensional confinement, an inhomogeneous offset field is generated by two conductors, T1 and T5 in Fig. 1(b), perpendicular to the waveguide ("transport wires"). The distance between T1 and T5 is $4d_T$. For identical currents I_T in T1 and T5, the magnetic field is described by its components

$$B_x=0,$$

$$B_y=\frac{\mu_0}{2\pi}I_T\left(\frac{2d_T+z}{(s_0+y_0)^2+(2d_T+z)^2}-\frac{2d_T-z}{(s_0+y_0)^2+(2d_T-z)^2}\right),$$

$$B_z = -\frac{\mu_0}{2\pi} I_T \left(\frac{s_0 + y_0}{(s_0 + y_0)^2 + (2d_T + z)^2} + \frac{s_0 + y_0}{(s_0 + y_0)^2 + (2d_T - z)^2} \right). \quad (6)$$

In our setup the transport wires are located at the back side of the substrate separated from the QP wires by s_0. The B_z component provides the overall nonvanishing offset field for the waveguide. Near the minimum of B_z, between T1 and T5, the potential is approximately parabolic, with an axial oscillation frequency ω_a [Eq. (10)] and an offset field value

$$B_{\text{off}} = \frac{\mu_0}{\pi} \frac{I_T (s_0 + y_0)}{(s_0 + y_0)^2 + 4d_T^2}. \quad (7)$$

The axial potential is plotted in Fig. 1(c). The field component B_y causes a small rotation of the waveguide about the y axis. The rotation angle at the bottom of the trap is estimated by

$$\alpha \approx -\frac{\mu_0}{\pi} \frac{I_T}{a_r} \frac{y_0^2 - 4d_T^2}{(y_0^2 + 4d_T^2)^2}. \quad (8)$$

The trapping potential generated by the five conductors QP1, QP2, QP3, T1, and T5 is characterized by the field curvatures b_i,

$$b_{\text{axial}} = \frac{\mu_0}{2\pi} I_T (s_0 + y_0) \frac{48d_T^2 - 4(s_0 + y_0)^2}{[(s_0 + y_0)^2 + 4d_T^2]^3},$$

$$b_{\text{radial}} = \frac{a_r^2}{B_{\text{off}}} = \frac{\mu_0}{2\pi} \frac{2I_{\text{QP2}}^2}{y_0^4 I_T (s_0 + y_0)} \frac{(s_0 + y_0)^2 + 4d_T^2}{[1 + (r_0/d_{\text{QP}})^2]^2}, \quad (9)$$

and the resulting trap frequencies ω_i, i=axial,radial,

$$\omega_i = \sqrt{\frac{g_F m_F \mu_B}{m} b_i}. \quad (10)$$

The above expressions assume infinite conductor lengths. The finite length of the conductors on the real chip (Fig. 4) results in a deviation of the axial and radial trap frequencies by 5 and 4 %, respectively.

The five-wire configuration achieves full, three-dimensional confinement of atoms using magnetic fields generated by the chip only. Precise control of the position (x_0, y_0) and parameters of the trap is therefore possible. The z position of the trap is controlled by further transport wires T1–T8. A trap generated by T1 and T5 will have identical parameters to one generated by T2 and T6 (Fig. 1). One trap can be continuously transformed into the other by reducing the current in one of the pairs while increasing it in the other. Thereby, the trap center shifts by d_T, the distance between two neighboring conductors T_{i} and $T_{\text{i+1}}$. While in general the axial trap frequencies change during the transport, we have calculated an optimum trajectory of the currents $I_{\text{T2}}(I_{\text{T1}})$, the same as for $I_{\text{T6}}(I_{\text{T5}})$, so that the axial trapping frequency remains constant.

On our chip the transport wires T_{i} are spaced by d_T=650 μm (Fig. 4). For a trap to be transported at constant height of about 300 μm, the optimum currents, fitted to third order, are

$$\frac{I_{\text{T2}}}{I_{\text{T}}} = 1 - 2.39\frac{I_{\text{T1}}}{I_{\text{T}}} + 2.31\left(\frac{I_{\text{T1}}}{I_{\text{T}}}\right)^2 - 0.92\left(\frac{I_{\text{T1}}}{I_{\text{T}}}\right)^3. \quad (11)$$

The axial displacement of the trap in terms of the currents is given by

$$z_0 = d_T \left[1 - 1.49\frac{I_{\text{T1}}}{I_{\text{T}}} + 0.49\left(\frac{I_{\text{T1}}}{I_{\text{T}}}\right)^2 \right]. \quad (12)$$

I_{T} is the initial current in T1 and T5. Keeping the axial trap frequency and the height above the chip constant by changing the currents in the transport wires as described above, the offset field and correspondingly the radial trap frequency would vary by a factor of 1.14 and 0.94, respectively. The variation of the radial trap frequency, however, can be compensated by varying the radial gradient [Eq. (4)] of the trap through matching the currents in the three quadrupole wires $I_{\text{QP1}} = I_{\text{QP3}}$ and I_{QP2} while holding the ratio $I_{\text{QP1}}/I_{\text{QP2}}$ constant. The latter condition is necessary for the constant height [Eq. (3)]. On the other hand, the transport wires produce a nonvanishing y component of the magnetic field at the trap center [Eq. (6)], altering the x position of the trap during the transport by ± 1.3 μm. This is in general a negligible effect, but can also be compensated by matching the currents I_{QP1} and I_{QP3} while keeping their sum constant. As a result, we are able to move the trap in the axial direction while keeping the radial and axial trap frequencies as well as the radial (x, y) position of the trap constant. The axial trapping potential is plotted in Fig. 3(a) during the optimized transport over a distance of d_T (solid line). The curvature of the potential near the minimum does not change, while a small change in the offset field is visible. During transport, the axial trap depth reduces to almost half of its initial and final values. Nonetheless, this does not set any relevant restrictions on experiments which are operated with sufficiently cold ensembles.

On our atom chip, we have integrated a set of eight conductors T1–T8 which repeat periodically over the length of the chip (see next section). Transport of atomic clouds is possible over a distance of 1.75 cm without any change of the trap frequencies or the radial position. The conveyor on our chip has been developed with respect to this scaleability, allowing coherent transport of condensates over a large distance. A Bose-Einstein condensate of interacting particles is a nonlinear medium sensitive even to nonresonant excitations [11], e.g., through changes of the trap frequencies. Coherent, excitationless transport of the condensate thus requires constant trap frequencies as provided by the conveyor belt described in this paper.

III. COMBINED CHIPS

In subsequent experiments, we have used a combined atom chip. This consists of a carrier chip, which operation principle has been outlined in the previous section, and several atom-optics chips.

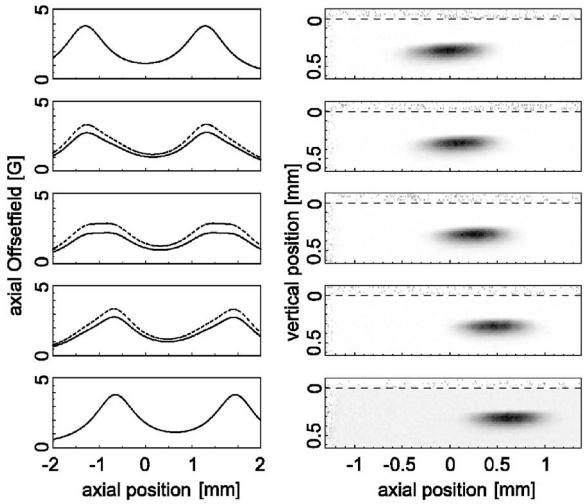

FIG. 3. (Left) The axial magnetic potential for five displacements (0, 162.5, 325, 487.5 and 650 μm) during transport over d_T=650 μm (solid line). Matching the currents in T1, T2, T4, and T5 [Eq. (11)] results in a smooth transport without changing the trap frequencies. (Right) Absorption images of thermal clouds for the corresponding displacements. The dashed line shows the chip surface. In this experiment the currents were driven linearly, resulting in a variation of the axial potential (dashed potential curves on the left).

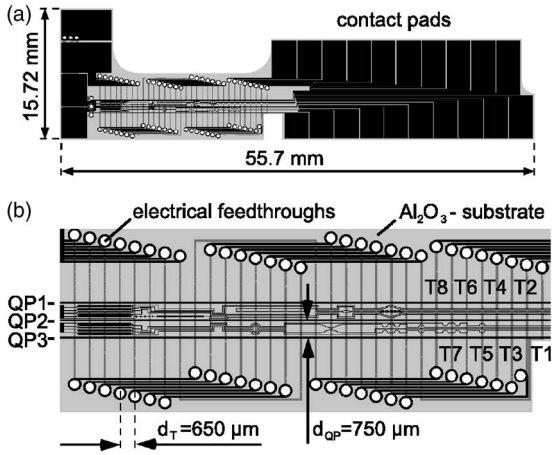

FIG. 4. Carrier chip. (a) Schematic plot of the dual-layer atom chip with conductors at both surfaces of the substrate and contact pads on the top. (b) Central part of the carrier chip. Indicated are the conductors QP1, QP2, and QP3 on the top and the transport wires T1–T8 on the back surface of the chip. The eight transport wires are periodically repeated underneath the chip. Electrical connection between the separate blocks of T1–T8 is achieved by running the wires through laser cut holes from underneath to the top surface of the chip and back. The additional wire pattern between QP1 and QP2, as well as between QP2 and QP3 are not used for the experiments described in this article. These can be used for further microtraps as described elsewhere [16].

A. Carrier chip

The carrier chip is a dual-layer atom chip which produces the entire magnetic field for three-dimensional magnetic trapping and manipulation of Bose-Einstein condensates (Fig. 4). It supports the QP and T wires described in the previous section. Additional wire patterns shown in Fig. 4 between QP1 and QP2 and between QP2 and QP3 were deposited for further microtraps, however, these are not used in the present work.

The chip was produced by electroplating gold conductors on both sides of a 250-μm-thick aluminium oxide substrate of size 15.7×55.7 mm. A tungsten-titanium alloy adhesive layer was used between the substrate and the gold wires. The conductors are 100 μm wide and 6 μm thick. Conductor lengths vary from 2.3 cm up to 6.5 cm. In a vacuum environment, the wires can sustain continuous currents of 1.35 A, corresponding to a current density of $j_{\max}=2.3\times10^5$ A/cm^2. In pulsed operation (3 s operation time, 60 s duty cycle), a maximum current of 2.8 A and a current density of $j_{\max}=4.7\times10^5$ A/cm^2 was achieved.

The conductors QP1, QP2, and QP3 are each separated by a distance of d_{QP}=750 μm. Conductors T1–T8 underneath the substrate are separated by d_T=650 μm and are repeated periodically over a distance of 20.15 mm. Crossings are avoided by running these from the underneath to the top of the substrate and back again. Contact is made through laser cut holes of 400 μm diameter and electroplating gold inside. Electrical contacts to macroscopic conductors are made via the 24 contact pads on the top of the substrate.

A typical trap we use for the preparation and manipulation of Bose-Einstein condensates of ^{87}Rb atoms in the $F=2, m_{\mathrm{F}}=2$ hyperfine ground state is generated by the currents $I_{\mathrm{QP1}}=I_{\mathrm{QP3}}=0.85\mathrm{A}, I_{\mathrm{QP2}}=0.235\mathrm{A}$, and $I_{\mathrm{T1}}=I_{\mathrm{T5}}=0.6\mathrm{A}$. This trap is located 300 μm above the surface of the chip, the trap frequencies are 140 Hz in the radial and 16 Hz in the axial direction. The trap depth is 87 μK in the radial and 108 μK in the axial direction. In this trap, no fragmentation of Bose-Einstein condensates is observed.

B. Atom-optics chips

Our atom-optics chips consist of micron-scaled conductors deposited on silicon substrates. High quality 300-nm-thick gold conductors have been patterned using standard techniques of electron-beam lithography and dry etching. Figures 5(a) and 5(b) show the microscope image and connection scheme of two nested meandering current patterns. The 1-μm-wide conductors are separated by 1-μm gaps. With 372 parallel conductor stripes, the structure has a total length of 743 μm and a width of 100 μm. Driven with currents as indicated in Fig. 5(c), a magnetic lattice potential [17–19] of 4 μm period is generated.

Atom-optics chips are attached to the carrier using ceramic glue [Fig. 5(a)]. The meandering current pattern sits approximately 250 μm above the surface of the carrier chip. The magnetic field of the meander can be superposed on the magnetic waveguide potential positioned above it.

Because of its large size, the carrier chip can host several atom optics chips, as depicted in Fig. 5(a). The electrical connection of atom-optics chips is realized by wire bonding to the carrier chip. Atomic clouds initially loaded into the magnetic potential of the carrier chip can be positioned over any of the atom-optics chips using the conveyor and the

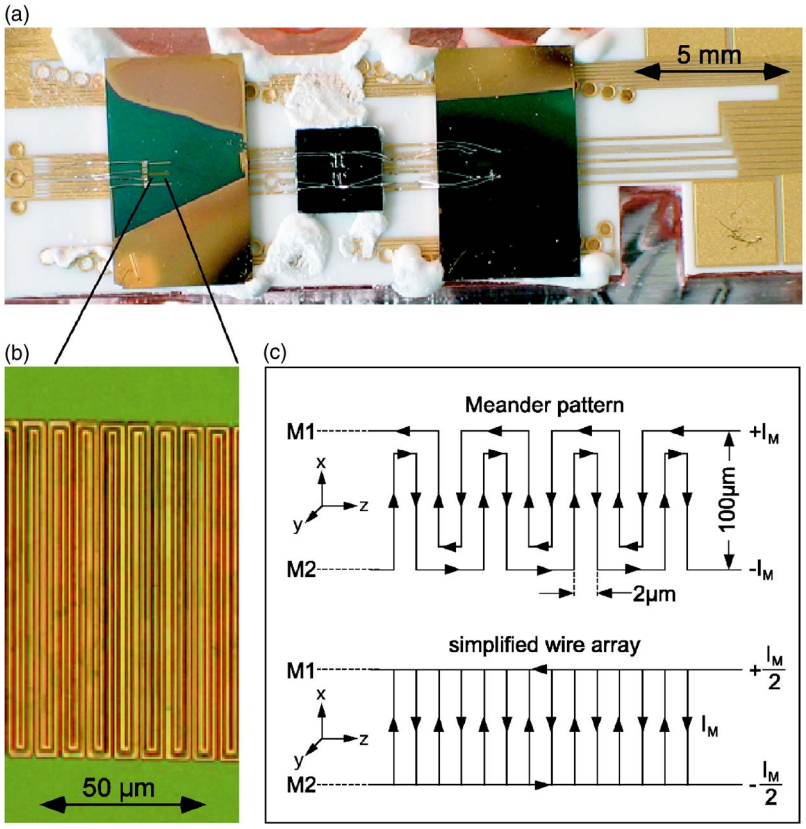

FIG. 5. (Color online) (a) Combined chip. Atom-optics chips with micron scaled conductor patterns are attached to the surface of the carrier chip. (b) Microscope image of a meandering conductor structure deposited on the atom-optics chip on the left. Conductors of 1 μm width are separated by gaps of 1 μm. (c) Schematics and connection scheme of the nested meander patterns M1 and M2. The simplified geometry (bottom) is used for calculating magnetic fields in the center area of the structure.

waveguide. Precise positioning of Bose-Einstein condensates on the atom-optics chips is described in Sec. IV.

IV. EXPERIMENTS ON THE CARRIER CHIP

A. Transport on conveyor

A key feature of the carrier chip is its ability to achieve smooth transport over distances, limited only by the length of the chip, in our experiment to 17.5 mm. Transport is demonstrated using a thermal cloud of 1.5×10^6 rubidium atoms at a temperature of 6 μK. The cloud is initially loaded into a trap as characterized in the last paragraph of Sec. III A. We begin the transport by accelerating the cloud over 500 ms to a velocity of v_T=2.6 mm/s. The acceleration is increased to a maximum value of $a_{\max}$=8.2 mm/s^2 and subsequently reduced to zero, both with a sinusoidal characteristic shape. During the 500 ms of acceleration, the trap moves by 650 μm along the z axis. Then the cloud moves with a constant velocity of v_T=2.6 mm/s and covers a distance of 650 μm in 250 ms. In the experiment shown in Fig. 6, the cloud was slowed down in 500 ms using the inverse acceleration ramp. The cloud arrives at rest (without sloshing) after travelling a total distance of 1.95 mm.

A thermal cloud is less sensitive to variations of the trap parameters so this transport was done with a simplified, linear relation between the currents $I_{T2}=I_T-I_{T1}$ instead of Eq. (11). The displacement is then approximated by a linear function of the currents in the transport wires, resulting in a relevant simplification of the computer program controling the experiment. However, this simplification means that the trap parameters change during the transport: the radial trap frequency decreases by up to 7 % and the axial frequency increases by up to 14 %. The dashed line in Fig. 3 (left) shows the axial potential shape for the simplified transport with respect to the exact scheme, shown as a solid line. Nevertheless, the transport takes place without any heating, since the atoms can follow the frequency changes adiabatically. Absorption images of the cloud taken every 50 ms for a total transport time of 1.25 s were fitted by a two-dimensional

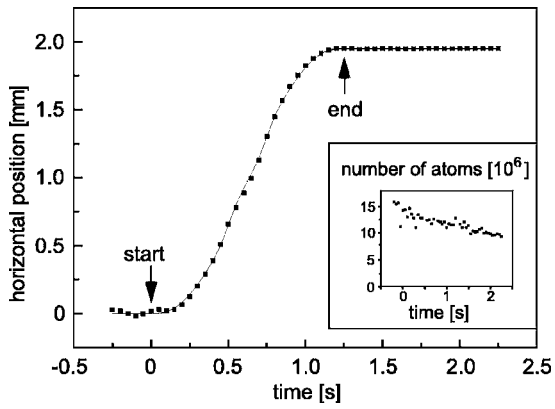

FIG. 6. Position of a thermal cloud during transport over a distance of 1.95 mm. The transport starts at t=0. The atoms are accelerated to a velocity of v_T=2.6 mm/s over 500 ms. For the next 250 ms the atoms move at constant velocity v_T before they are decelerated within another 500 ms until they come to rest at t=1.25 s. The solid line shows the expected position, calculated from the currents in the wires. The inset image shows the number of atoms estimated from the absorption images changing in time.

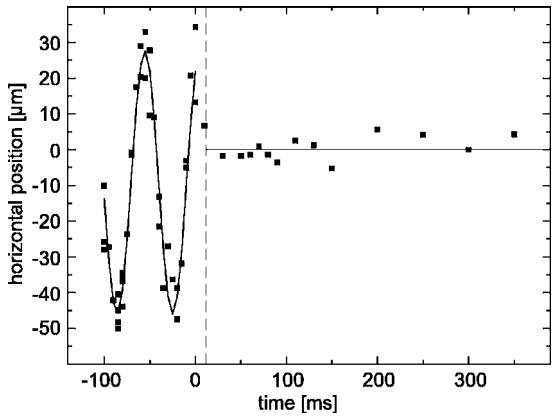

FIG. 7. Eliminating axial center-of-mass oscillations of a Bose-Einstein condensate. Axial position of a condensate, initially oscillating with $\omega=2\pi\times(16.4\pm0.3)\mathrm{s}^{-1}$ and $A=(36.8\pm1.6)\mu$m, after 25 ms time of flight. The center-of-mass motion is stopped by a phase-matched displacement of the trap center using the conveyor.

Gaussian function in order to determine the number of atoms, temperature, and position. The five absorption images in Fig. 3 show the acceleration period of the transport (first 500 ms), while in Fig. 6 the measured position of the cloud center (filled squares) as well as its numerically calculated value (solid line) is plotted for the duration of the transport (1.25 s). The data and a calculation based on the current slopes show excellent agreement. The inset of Fig. 6 shows the number of atoms in the trap over the transport period. No relevant loss related to the transport is observed. A slow evaporation and reduction of temperature is observed, which we attribute to the reduced trap depth during transport.

In most cases, it is preferable to transport thermal clouds, and subsequently generate condensates in the microtrap where further experiments are to be performed. This way, no density dependent losses or nonlinear excitations of the condensate are present during the transport. Additional micron-scaled positioning can be done after producing the condensate. This is necessary when a condensate has to be positioned a few microns from the surface, as the radius of a thermal cloud exceeds this distance.

B. Position and momentum control of condensates

The carrier chip can be used for submicron positioning and momentum control of the condensate. We demonstrate this by showing that an initially sloshing condensate can be brought to rest by carefully displacing the trap. A small amplitude (harmonic) oscillation is first induced on the trapped condensate,

$$z(t) = A\,\sin(\omega_a t + \phi) + z_0. \tag{13}$$

The phase and amplitude of the oscillation are detected after 25 ms time-of-flight (Fig. 7). As the imaged cloud position depends on both its position and momentum at the time the trap is turned off, the data is fitted by the function

$$Z(t) = A\,\sin(\omega_a t + \phi) + A\omega_a\tau\cos(\omega_a t + \phi) + z_0, \tag{14}$$

describing the position of the oscillating cloud after τ time of flight. The fit parameters $A=(15.8\pm0.8)\ \mu\mathrm{m}, \omega=2\pi\times(16.4\pm0.3)\ \mathrm{s}^{-1}$, and $\phi=(-0.014\pm0.09)$ are used to determine the magnitude and timing of the trap displacement required to stop the oscillation. Radial excitations are avoided if the displacement is applied on a time scale longer than the radial oscillation period. The displacement is initiated 5 ms prior to when the center of mass motion reaches its turning point. Within 10 ms the trap is displaced by 16 μm along z, and the cloud arrives at rest (Fig. 7). Based on the accuracy of the current sources used for the experiment [20], it is in principle possible to calculate the trap position to a few nm [21]. The accuracy of our measurement, however, is limited by the optical resolution of the imaging system which is approximately 5μm.

V. EXPERIMENTS ON ATOM-OPTICS CHIPS

A. Positioning condensates on micron scaled atom-optics chips

The time-of-flight position of a Bose-Einstein condensate is determined by the motion of the cloud after the trapping potential is turned off. Spin polarized atomic clouds in a magnetic-field sensitive state are accelerated not only by gravity but also by magnetic-field gradients. The method we describe for positioning Bose-Einstein condensates on the micron-scaled atom-optics chips exploits the change in position of the condensate, after being exposed to the magnetic field of the microstructured electromagnets, during the time of flight. The field adds to ambient stray magnetic fields in the laboratory and changes the trajectories of released clouds. In a series of experiments, the initial position of the condensate can be varied and the magnetic field of the atom-optics chip mapped out by comparing the position after ballistic expansion with and without current in the electromagnets.

The method is demonstrated for an atom-optics chip with a known meandering current pattern (Fig. 5). Using the carrier chip, condensates were positioned at constant y and z, but different x positions below the chip. At each horizontal position, the distance to the surface was calibrated by moving the condensate towards the chip surface, until it was lost due to atom-surface interactions. During positioning, the meandering current was turned off. For each initial x position, the vertical position (y) of the condensate was detected after 25 ms time of flight with zero and ±1 mA current in the meander. The current was applied during the first 5 ms of the ballistic expansion. Because the imaging beam propagates parallel to the x axis, only displacements along y and z were detectable. Measurements in the center area of the meander reveal only vertical y displacements. The displacements plotted in Fig. 8 are relative to the time-of-flight position for zero current. Although the cloud was only shifted parallel to the imaging beam, we were able to accurately detect the 100 -μm-wide feature of the meander. Due to the finite width of the pattern (100 μm), the characteristics are dominated by the magnetic field of currents at the edge of the meander (see Fig. 5, simplified wire array) while the contribution of the

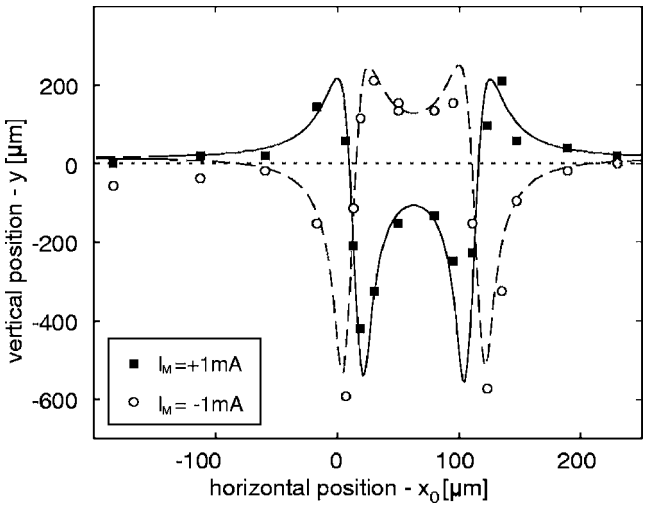

FIG. 8. Positioning condensates on a meandering wire pattern. Plot of the position of Bose-Einstein condensates after 25 ms ballistic expansion for currents $I_M=+1$mA (solid squares) and $I_M=-1$ mA (open circles) in the meandering current path, relative to the position for zero current. The current was applied during the first 5 ms of the time of flight. The data are compared to the numerical integration of the equation of motion, based on the known structure of the meander pattern (solid and dashed lines).

periodic pattern with alternating currents is negligible for distances larger than the period [18]. The asymmetry for positive and negative currents is due to ambient magnetic fields.

The data are compared to the numerical integration of the equation of motion for rubidium atoms in this magnetic field. The simultaneous fit to both data sets, for 1 and -1 mA, gives the center position of the meander structure to be shifted by $x_0=62.58\pm1.37$ μm relative to the origin which was defined to be the center of the conductor QP2 on the carrier chip. The fit also gives the distance to the chip surface $y_0=14.00\pm1.55$ μm and the ambient magnetic fields $(B_x\approx0G, B_y\approx1G, B_z\approx1.9G)$.

The same method is applicable for measuring the position of the meandering current pattern along the z coordinate. Calibration curves such as in Fig. 8 allow the ultraprecise, three-dimensional positioning of condensates on micron-scaled atom-optics chips.

B. Direction sensitive magnetic field microscope

We now describe the principle of a magnetic-field microscope based on the controlled translation of a well-known magnetic potential. Bose-Einstein condensates are used as tiny probes, for measuring the difference between the applied and the actual potential. The microscope is demonstrated by mapping the magnetic field of a 1-μm-wide test conductor.

The potential experienced by the condensate can be decomposed into a well-known trapping potential $U_0(z)$ and an unknown potential $U_1(z)$ to be measured:

$$U(z)=U_0(z)+U_1(z). \tag{15}$$

The potential $U_0(z)$ is related to the axial confinement of our waveguide on the carrier chip,

$$U_0(z)=\frac{1}{2}m\omega^2(z-z_0)^2. \tag{16}$$

At the minimum z_i of the potential $U(z)$, the first derivative of $U(z)$ vanishes and

$$\left.\frac{dU_1(z)}{dz}\right|_{z_i}=-\left.\frac{dU_0(z)}{dz}\right|_{z_i}=-m\omega^2(z_i-z_0) \tag{17}$$

with z_0 being the minimum of U_0.

According to Eq. (17), the gradient of $U_1(z_i)$ is proportional to the difference (z_i-z_0). From this difference, the magnetic-field distribution of the sample can be derived. By translating the center z_0 of the well-known potential $U_0(z)$ and detecting the position z_i where a Bose-Einstein condensate is localized, the gradient of U_1 can be measured as a function of z_i. Note that the potential $U(z)$ can have several minima z_i, $(i=1, 2,\ldots)$. Integration of Eq. (17) over z gives the potential $U_1(z)$.

The realization of this microscope requires the potential $U_0(z)$ to be well known. It must also be possible to precisely shift its position which is possible with the microstructured conveyor belt of the carrier chip described in Sec. II. Keeping the x and y coordinates constant is essential for the measurement. Keeping also the axial oscillation frequency ω_a constant simplifies the analysis. The conveyor belt and manipulation schemes described in this paper easily meet these requirements. Through the three-dimensional position control of Bose-Einstein condensates on the carrier chip, a three-dimensional, highly sensitive measurement of the independent magnetic-field components is possible. This in turn allows the complete mapping of unknown magnetic potentials.

We demonstrate the microscope by measuring the z component of a 1-μm-wide, 300-μm long microstructured conductor aligned parallel to the x axis. The conductor was patterned on the surface of an atom-optics chip, the same as used for the meandering pattern. Experiments were carried out 390 μm away from the carrier chip in a smooth waveguide potential with an axial oscillation frequency of 16 Hz. Bose-Einstein condensates were positioned at different z positions around the thin conductor, and the position z_i was detected for a current of 1.2 mA, and z_0 for a current zero, as shown in Fig. 9(a). The position difference taken as a function of z_i was integrated to find the magnetic-field curve, Fig. 9(b), of the single conductor. The solid line is the calculated field of a finite length wire located 140 μm below the condensate. The sensitivity of the microscope can be calculated with Eq. (17) and depends only on the trap frequency and the resolution of the imaging system. With a reasonably low trap frequency of 1 Hz and an optical resolution of 1 μm a sensitivity of about 6.2×10^{-5} G/cm should be possible. In our experiment with $\omega_a=2\pi\times16$ s^{-1}, and an optical resolution of 5 μm, the sensitivity was 0.08 G/cm.

VI. CONCLUSIONS

We have presented experiments using a combined atom chip which allows one to work a few microns from a surface.

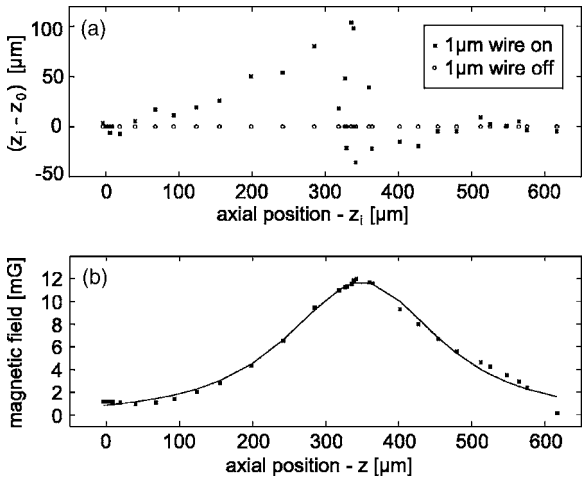

FIG. 9. (a) Magnetic-field microscope. Positions z_0 (open circles) and z_i (filled squares) of the Bose-Einstein condensate for zero and for 1.2 mA current, respectively, in a thin conductor perpendicular to the waveguide. (b) z component of the magnetic field of the thin conductor, as integrated from the measured gradient according Eq. (17). The data are in good agreement with the axial field component calculated for a finite wire oriented parallel to the x axis.

Fragmentation is avoided because the waveguide potential is formed by conductors at large distances from the condensate. Johnson-noise-induced spin-flip losses are greatly reduced as the only conductor in close proximity is a narrow wire aligned transverse to the cloud [22]. The described methods here provide a route towards micron-scale atom optics.

We have also performed experiments in which condensates were loaded into a magnetic lattice produced by the meandering current pattern. While interference following release from these traps was observed [23], the (exponential) height dependence of the lattice leads to a highly complex situation. This contrasts with optical standing waves where the lattice potential is homogeneous over the size of the condensate. It therefore remains an experimental challenge to engineer advanced atom-optical elements with magnetic potentials for extended clouds of Bose-Einstein condensates. Many of the proposed advantages of atom chips, however, such as precisely controlled tunnelling rates through potential barriers and in lattices should be attainable using smaller wave packets or single atoms.

ACKNOWLEDGMENTS

This work was supported by the Deutsche Forschungsgemeinschaft, Landesstiftung Baden-Württemberg, EU Marie-Curie RTN on Atomchips, and the Australian Research Council. The authors thank D. Kölle, R. Kleiner (Physikalisches Institut, Universität Tübingen), and C. Dücsö (MFA/KFKI) for production of microchips.

[1] J. D. Weinstein and K. G. Libbrecht, Phys. Rev. A **52**, 4004 (1995).
[2] A. Smerzi, S. Fantoni, S. Giovanazzi, and S. R. Shenoy, Phys. Rev. Lett. **79**, 4950 (1997).
[3] T. Paul, K. Richter, and P. Schlagheck, Phys. Rev. Lett. **94**, 020404 (2005).
[4] U. Dorner, P. Fedichev, D. Jaksch, M. Lewenstein, and P. Zoller, Phys. Rev. Lett. **91**, 073601 (2003).
[5] H. Ott, J. Fortágh, G. Schlotterbeck, A. Grossmann, and C. Zimmermann, Phys. Rev. Lett. **87**, 230401 (2001).
[6] W. Hänsel, P. Hommelhoff, T. W. Häansch, and J. Reichel, Nature (London) **413**, 498 (2001).
[7] C. Henkel, S. Pötting, and M. Wilkens, Appl. Phys. B: Lasers Opt. **69**, 379 (1999).
[8] M. P. A. Jones, C. J. Vale, D. Sahagun, B. V. Hall, C. C. Eberlein, B. E. Sauer, K. Furusawa, D. Richardson, and E. A. Hinds, J. Phys. B **37**, L15 (2004).
[9] J. Estève, C. Aussibal, T. Schumm, C. Figl, D. Mailly, I. Bouchoule, C. I. Westbrook, and A. Aspect, Phys. Rev. A **70**, 043629 (2004).
[10] S. Kraft, A. Günther, H. Ott, D. Wharam, C. Zimmermann, and J. Fortágh, J. Phys. B **35**, L469 (2002).
[11] H. Ott, J. Fortágh, S. Kraft, A. Günther, D. Komma, and C. Zimmermann, Phys. Rev. Lett. **91**, 040402 (2003).
[12] C. Henkel, P. Krüger, R. Folman, and J. Schmiedmayer, Appl. Phys. B: Lasers Opt. **76**, 173 (2003).
[13] R. Folman, P. Krüger, J. Schmiedmayer, J. Denschlag, and C. Henkel, Adv. At., Mol., Opt. Phys. **48**, 263 (2002).
[14] C. V. Sukumar and D. M. Brink, Phys. Rev. A **56**, 2451 (1997).
[15] D. E. Pritchard, Phys. Rev. Lett. **51**, 1336 (1983).
[16] S. Kraft, A. Günther, P. Wicke, B. Kasch, C. Zimmermann, and J. Fortágh, cond-mat/0504242 (unpublished).
[17] D. C. Lau, A. I. Sidorov, G. I. Opat, R. J. McLean, W. J. Rowlands, and P. Hannaford, Eur. Phys. J. D **5**, 193 (1999).
[18] D. C. Lau, R. J. McLean, A. I. Sidorov, D. S. Gough, J. Koperski, W. J. Rowlands, B. A. Sexton, G. I. Opat, and P. Hannaford, J. Opt. B: Quantum Semiclassical Opt. **1**, 371 (1999).
[19] L. Cognet *et al.*, Europhys. Lett. **47**, 538 (1999).
[20] URL http://www.highfinesse.de/steuer_1.html
[21] P. Hommelhoff, W. Hänsel, T. Steinmetz, T. W. Hänsch, and J. Reichel, New J. Phys. **7**, 3 (2005).
[22] C. Henkel and S. Pötting, Appl. Phys. B: Lasers Opt. **72**, 73 (2001).
[23] A. Günther, S. Kraft, M. Kemmler, D. Kölle, R. Kleiner, C. Zimmermann, and J. Fortágh, cond-mat/0504210 (unpublished).